

Electronic Structure of Epitaxial Films of the Bilayer Strontium Ruthenate: $\text{Sr}_3\text{Ru}_2\text{O}_7$

Sethulakshmi Sajeev,¹ Arnaud P. Nono Tchiomo,¹ Brendon Faeth,^{2,3} Evan Krysko,^{2,3} Olivia Peek,^{2,4} Matthew J. Barone,^{2,3} Jordan Shields,⁵ Neha Wadehra,^{2,3} Garu Gebreyesus,⁶ Divine Kumah,⁵ Richard M. Martin,⁷ Darrell G. Schlom,^{2,3} and Prosper Ngabonziza^{1,8,*}

¹*Department of Physics & Astronomy, Louisiana State University, Baton Rouge, LA 70803, USA*

²*Platform for the Accelerated Realization, Analysis, and Discovery of Interface Materials(PARADIM), Cornell University, Ithaca, New York, 14853, USA*

³*Department of Material science and engineering, Cornell University, Ithaca, New York, 14853, USA*

⁴*Department of Physics, Cornell University, Ithaca, New York, 14853, USA*

⁵*Department of Physics, Duke University, Durham, North Carolina*

⁶*Department of Physics, College of Basic and Applied Sciences, University of Ghana, Ghana*

⁷*Department of Applied Physics, Stanford University, Stanford, California 94305, USA*

⁸*Department of Physics, University of Johannesburg, P.O. Box 524 Auckland Park 2006, Johannesburg, South Africa*

(Dated: February 10, 2026)

We report the first combined study of the low-energy electronic band structure of epitaxial $\text{Sr}_3\text{Ru}_2\text{O}_7$ films using angle-resolved photoemission spectroscopy (ARPES) and density functional theory (DFT). The complete Fermi-surface topography of the near-Fermi-level bands is determined from in-situ ARPES measurements. To investigate the effects of substrate-induced strain on the band structure, $\text{Sr}_3\text{Ru}_2\text{O}_7$ thin films are epitaxially grown on SrTiO_3 (STO) and $(\text{LaAlO}_3)_{0.3}(\text{Sr}_2\text{TaAlO}_6)_{0.7}$ (LSAT) substrates using molecular beam epitaxy. The combination of the measured Fermi-surfaces along with the theoretical interpretation, clearly show dramatic changes in the Fermi surface topologies that result from the underlying strain states of the films on the two substrates. We find that the $\text{Sr}_3\text{Ru}_2\text{O}_7$ films prepared on STO are tensile strained with tetragonal symmetry, whereas those grown on LSAT are compressively strained with orthorhombic symmetry. Within ~ 15 meV below the Fermi level, we observe two flat bands along Γ - X in the orthorhombic phase and around Γ in the tetragonal phase. These features could be favorable for van Hove singularities near the Fermi level, and highlight the emergence of magnetic instabilities in epitaxial $\text{Sr}_3\text{Ru}_2\text{O}_7$ films.

Ruthenium oxides of the Ruddlesden-Popper (R-P) phases, $\text{Sr}_{n+1}\text{Ru}_n\text{O}_{3n+1}$ ($n = 1, 2, 3, \infty$), are a class of strongly correlated materials that have garnered significant attention because they feature several comparable interactions that compete to engender a variety of novel electronic and magnetic phenomena [1–5]. The vast collection of ground-state properties in this series includes unconventional superconductivity in Sr_2RuO_4 ($n = 1$) [1, 2], the quantum critical metamagnetism and nematicity in $\text{Sr}_3\text{Ru}_2\text{O}_7$ ($n = 2$) [3, 6], anisotropic ferromagnetism and proposed orbital-dependent metamagnetism in $\text{Sr}_4\text{Ru}_3\text{O}_{10}$ ($n = 3$) [4, 7] and the spontaneous itinerant ferromagnetism in SrRuO_3 ($n = \infty$) [5]. The richness of different phenomena in Sr-based layered ruthenates comes from a competition between local and itinerant electronic behaviors. This involves a strong interplay between charge, spin, orbital, and lattice degrees of freedom, which underlie the complex ground states and responses of these materials to external perturbations [8, 9]. All the above ground-state properties demonstrate that the $\text{Sr}_{n+1}\text{Ru}_n\text{O}_{3n+1}$ materials provide a fascinating platform for exploring diverse novel quantum phenomena in correlated ruthenate systems.

The focus of this paper is on the bilayer strontium ruthenate system $\text{Sr}_3\text{Ru}_2\text{O}_7$. It is a quasi-two-

dimensional material due to the strong interactions of the Ru-O layers within the bilayer in the ab -plane, and the weaker interactions between adjacent bilayers along the c -axis [10]. The crystal symmetry of $\text{Sr}_3\text{Ru}_2\text{O}_7$ is commonly described as tetragonal, with space group $I4/mmm$ [see, Fig. 1(a)]. However, structural refinements based on neutron and x-ray diffraction have revealed an in-plane rotation of the RuO_6 octahedra by approximately 7°, which lowers the symmetry [11, 12]. As a result, some studies report an orthorhombic structure, assigning space groups such as $Bbcb$ or $Pban$, depending upon the specific modeling and refinement conditions [11–15].

$\text{Sr}_3\text{Ru}_2\text{O}_7$ is a strongly enhanced Pauli paramagnet in its ground state, but undergoes a field-induced metamagnetic transition at temperatures as low as 5 K, characterized by a rapid and superlinear increase in magnetization. This metamagnetic behavior is accompanied by pronounced anomalies in thermodynamic and transport properties, including divergences in the electrical resistivity and the electronic specific heat near critical magnetic field values [16–20]. These strong fluctuations have been widely discussed within phenomenological frameworks invoking a putative metamagnetic quantum critical end point [17, 18, 21, 22].

There have also been studies suggesting that the microscopic origin of the metamagnetism in $\text{Sr}_3\text{Ru}_2\text{O}_7$ lies in the electronic band structure. For instance, theoretical works and band structure calculations proposed that the phase diagram of $\text{Sr}_3\text{Ru}_2\text{O}_7$ could be understood considering a Stoner-like model, where the resulting Fermi surface (FS) pocket derived from the Ru d_{xy} orbitals exhibits a nearby van Hove singularity in the density of states (DOS) [13, 23–25]. The predicted FS pockets of $\text{Sr}_3\text{Ru}_2\text{O}_7$ have been experimentally observed in angle resolved photoemission spectroscopy (ARPES) measurements performed on single crystals [26]. Upon careful characterization of the band dispersions near the Fermi level (E_F), it was found that the d_{xy} band presents saddle points and sharp peaks in the DOS, situations that are favorable for the occurrence of a van Hove singularity [26]. More importantly, the fact that these observations were made within an energy range consistent with the theoretical prediction of the Zeeman splitting for the metamagnetic transition [24] strengthens the idea that this emergent phenomenon in $\text{Sr}_3\text{Ru}_2\text{O}_7$ can be directly traced to the detailed structure of its FS.

Consequently, the electronic band structure and the FS topology of $\text{Sr}_3\text{Ru}_2\text{O}_7$ have been significantly investigated using both DFT calculations and ARPES [13, 27, 28]. So far, these studies have focused on $\text{Sr}_3\text{Ru}_2\text{O}_7$ in its single crystal form. To gain more insight into the microscopic origin of the magnetic instability, it could be advantageous to explore the band structure and FS of thin film samples. Unlike single-crystals, thin films offer the opportunity to explore interfacial effects, and tailor the properties of the material based on strains induced by the substrates on which they are grown [29].

Any modification of the Fermi surface (FS) induced by strain, whether subtle or pronounced, is expected to influence the dynamics of magnetic-field-controlled instabilities and may give rise to new phases [16, 28, 30, 31]. Changes in the FS topology arise from alterations of the underlying crystal symmetry, allowing strain engineering to provide precise control over the electronic and magnetic interactions in bilayered $\text{Sr}_3\text{Ru}_2\text{O}_7$ [26, 32, 33]. This tunability offers a powerful platform for exploring electronic and magnetic ordered phases, quantum criticality, and their relationship to the underlying band structure [31, 33, 34].

In particular, the strong sensitivity of $\text{Sr}_3\text{Ru}_2\text{O}_7$ to small structural, electronic, or magnetic perturbations makes it an ideal system for examining how subtle modifications of lattice symmetry or orbital hybridization reshape the FS and stabilize or suppress competing ground states [18, 32]. Such control not only advances our understanding of correlated 4d electron systems but also opens pathways for engineering novel quantum phases through targeted modifications of the crystal environment. More broadly, strain engineering has proven effective for enhancing electronic and magnetic properties

across materials, enabling improved photocatalytic and optoelectronic performance as well as controlled magnetic anisotropy in thin films [35–37]. However, electronic band-structure studies of epitaxial $\text{Sr}_3\text{Ru}_2\text{O}_7$ remain limited by the challenges of controlling layered-ruthenate epitaxy and achieving phase-pure thin films [29, 38, 39].

Here, we report the first combined experimental and theoretical investigation of the electronic band structure and FS topology of $\text{Sr}_3\text{Ru}_2\text{O}_7$ thin films. Using molecular beam epitaxy (MBE), we deposited $\text{Sr}_3\text{Ru}_2\text{O}_7$ films on LSAT and STO single-crystal substrates. The reflection high-energy electron diffraction (RHEED) data acquired during growth indicate high-quality epitaxial $\text{Sr}_3\text{Ru}_2\text{O}_7$ films; while the in-plane lattice parameters extracted from reciprocal space maps (RSMs) confirm coherent growth accompanied by compressive and tensile strains on LSAT and STO, respectively. To examine how these strain states modify the electronic structure, we performed ARPES measurements on the $\text{Sr}_3\text{Ru}_2\text{O}_7$ films. We observe substantial strain-dependent transformations in the band dispersions. The measured FSs show that compressively strained films adopt an orthorhombic structure, whereas tensile-strained films exhibit a tetragonal symmetry. These observations indicate that the RuO_6 octahedral rotation responsible for Brillouin zone reconstruction and band backfolding is suppressed in samples grown on STO. The DFT-calculated bands, obtained by incorporating the RSM-derived lattice parameters, are in general agreement with the ARPES experiments and reproduce the main features of the measured FSs. Within a few meV below E_F , we observe two flat bands along Γ -X in the orthorhombic phase and around Γ in the tetragonal phase. These bands suggest possible van Hove singularities near E_F , a condition that favors magnetic instabilities in epitaxial $\text{Sr}_3\text{Ru}_2\text{O}_7$ films.

To grow the $\text{Sr}_3\text{Ru}_2\text{O}_7$ thin films, the LSAT and STO substrates were kept at the optimal temperature of 625 °C, and the oxygen partial pressure in the growth chamber was maintained at 1.42×10^{-6} Torr. The procedure for the synthesis of the $\text{Sr}_3\text{Ru}_2\text{O}_7$ films with high phase purity is described elsewhere [40]. For this study, LSAT with lattice parameter $a = b = 3.868 \text{ \AA}$ [15, 41] and STO with lattice parameter $a = b = 3.905 \text{ \AA}$ [15, 42] were chosen for controlled strain engineering, since their relatively small lattice mismatch with $\text{Sr}_3\text{Ru}_2\text{O}_7$ ($a = b = 3.890 \text{ \AA}$) [11] yields respectively compressive and tensile strains in the film.

In-situ ARPES experiments were conducted at the temperature of 7 K, using a state-of-the art high-resolution Scienta DA-30L electron analyzer with an energy resolution of 5 meV. Figure 1(b) shows the angle-resolved geometry of the ARPES experiment. For these measurements, 6 nm thick $\text{Sr}_3\text{Ru}_2\text{O}_7$ samples were used. This was the optimal thickness ensuring high surface quality for the acquisition of high quality ARPES data. The theoretical investigations were carried out using

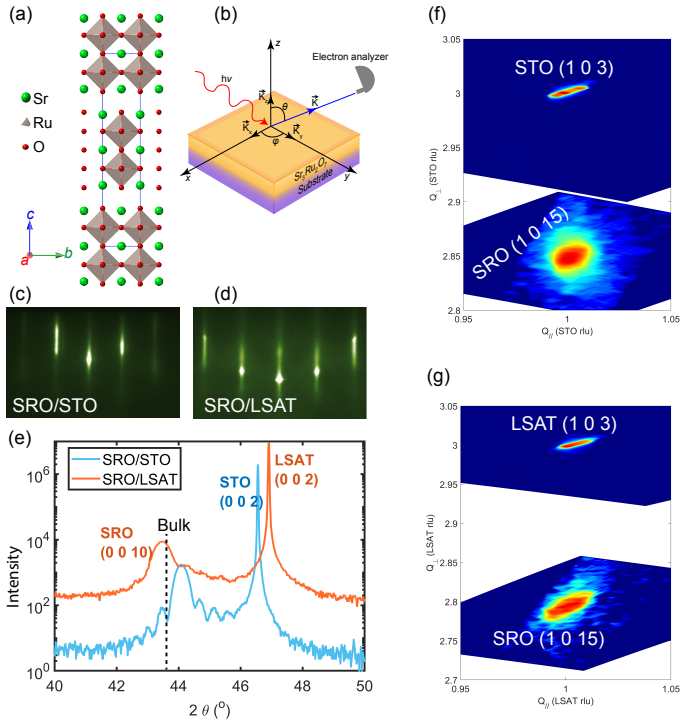


FIG. 1. (a) crystal structure of bilayered ruthenate $\text{Sr}_3\text{Ru}_2\text{O}_7$ in the tetragonal $I4/mmm$ phase. The blue contour encompasses the unit cell. (b) Schematic of the photoexcitation process in ARPES experiments viewed from the sample surface. The emission angle, θ , the sample rotation angle, φ , and the photoelectron wave vector, \vec{K} , are indicated. (c) and (d) RHEED images of $\text{Sr}_3\text{Ru}_2\text{O}_7$ (SRO) grown on STO and LSAT along (110) and (100) directions, respectively. (e) Close up view of XRD θ - 2θ scans of representative samples of thickness 18 nm (on LSAT) and 24 nm (on STO), around the (002) and (0010) reflections of the substrates and SRO films, respectively. The vertical dashed line indicates the position of the (0010) reflection for a fully relaxed SRO film. (f) and (g) Reciprocal space maps around (103) peaks of the substrates and (1015) peaks of the SRO films grown on STO and LSAT, respectively.

pseudopotential, plane-wave implementation of DFT as described in Ref. [7, 43].

The growth of the $\text{Sr}_3\text{Ru}_2\text{O}_7$ thin films was monitored in real time using RHEED. The diffraction patterns of the films grown on LSAT and STO are shown in Fig. 1(c) and 1(d), respectively. These patterns indicate good film quality and the epitaxial growth. In particular, the presence of the very sharp diffraction spots attests to the two dimensional growth mode of the $\text{Sr}_3\text{Ru}_2\text{O}_7$ films on both substrates, as well as to the flatness, the smoothness, and the perfect single crystalline structure of their surfaces [39, 44, 45].

The high crystalline quality of the $\text{Sr}_3\text{Ru}_2\text{O}_7$ films are further demonstrated in the structural data of representative films, presented in Fig. 1(e) - (g). The enlargement of θ - 2θ scans around the (0010) film peaks and the

(002) substrate planes underlines the presence of Kiessig fringes [Fig. 1(e)]. These interference fringes highlight the high structural quality of the surfaces and the well defined interfaces [46]. The c -axis lattice parameter values extracted from these scans are 20.792 Å and 20.512 Å, for the samples grown on LSAT and STO, respectively. Compared with the reported bulk value of 20.719 Å [11], these values are consistent with both the vertical elongation and compression of the RuO_6 octahedra associated with the in-plane compressive and tensile strains induced in the films by the LSAT and STO substrates, respectively [47].

Figures 1(f) and 1(g) show the reciprocal space maps around the (1015) Bragg reflections of the $\text{Sr}_3\text{Ru}_2\text{O}_7$ films prepared on STO and LSAT, respectively. These maps indicate coherent epitaxial growth and fully strained films on both substrates, consistent with previous reports [29, 38, 48]. For scans around the (0115) as well as the (0115) reflections, slightly different in-plane lattice parameters were obtained, especially for the films grown on LSAT. This would suggest an in-plane orthorhombicity for these films. However, given the limited resolution of the lab-based XRD system used for this study, these differences may fall within experimental errors, and could more conclusively be confirmed with high-resolution synchrotron measurements [49, 50]. Nevertheless, as will be discussed below, the orthorhombicity was incorporated into the FS calculations of the $\text{Sr}_3\text{Ru}_2\text{O}_7$ films grown on LSAT, yielding good agreement with the measured data.

Strain, interfacial coupling and film thickness have been shown to induce rotations of the RuO_6 octahedra in Sr-based ruthenate films, leading to modifications in both the underlying crystal symmetry and functional properties of the films [49–53]. In the following paragraphs, we examine how compressive and tensile strains alter the electronic band structures of $\text{Sr}_3\text{Ru}_2\text{O}_7$ films and analyze the extent to which these changes correlate with strain-driven structural phase transitions associated with octahedral rotations.

Figure 2 presents the experimental and calculated FSs of $\text{Sr}_3\text{Ru}_2\text{O}_7$ thin films prepared on both substrates. For the 6 nm thick film grown on LSAT [Fig. 2(a)], reasonable agreement is found with those of the orthorhombic $\text{Sr}_3\text{Ru}_2\text{O}_7$ single crystal [26], although not all the predicted surface pockets are resolved in our experimental data. The square and cross shaped hole-like FS pockets (α_1 , α_2) originating from the d_{xz} and d_{yz} orbitals are clearly identifiable. The electron pockets γ_1 and β at the M point, as well as the innermost δ sheet at the Γ point, are only weakly resolved in the ARPES data. A broad, high-intensity feature spanning the region near the X point is also observed, which may correspond to the small FS pocket labeled γ_2 in orthorhombic $\text{Sr}_3\text{Ru}_2\text{O}_7$ [26, 54]. The limited visibility of these small pockets is expected in epitaxial thin films, where reduced out-of-plane coher-

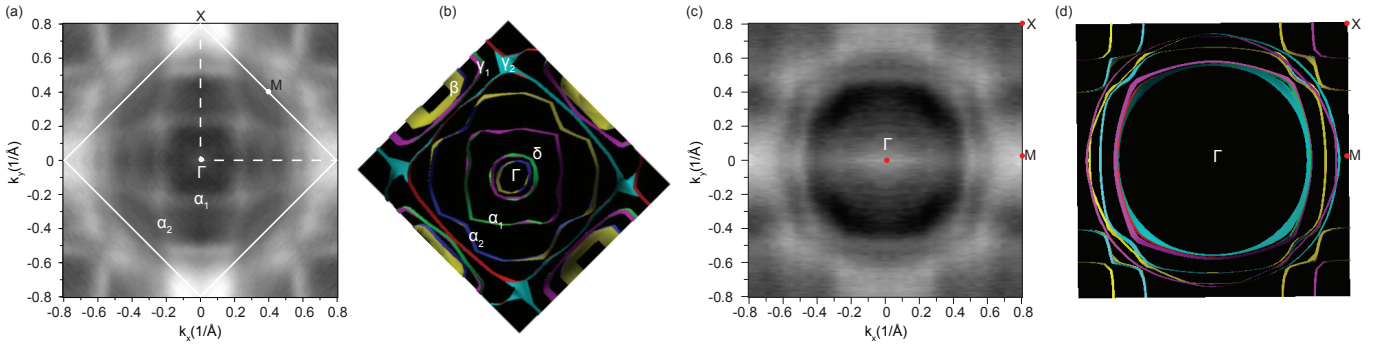


FIG. 2. (a) Symmetrized ARPES Fermi-surface map of $\text{Sr}_3\text{Ru}_2\text{O}_7$ grown on LSAT. The white square marks the reconstructed Brillouin zone arising from octahedral rotations. (b) Calculated Fermi surface of $\text{Sr}_3\text{Ru}_2\text{O}_7$ for LSAT-induced strain, which drives the system into an orthorhombic structure. (c) ARPES Fermi-surface map of $\text{Sr}_3\text{Ru}_2\text{O}_7$ grown on STO. (d) Calculated Fermi surface of $\text{Sr}_3\text{Ru}_2\text{O}_7$ under STO-induced strain resulting in a tetragonal phase.

ence, substrate-induced disorder, and strain-driven octahedral distortions broaden the spectral features, particularly for low-spectral-weight or symmetry-sensitive bands [55, 56].

The calculated FS [Fig. 2(b)] reproduces the main features observed in the measurements, including Brillouin-zone folding due to the doubled periodicity, the structural distortion inferred from the RSM analysis (orthorhombicity), and the effects of spin-orbit coupling. The latter likely explains the emergence of the δ pocket, whose orbital character is primarily e_g , which is typically unoccupied in the single-layer ruthenate, but exhibits substantial hybridization with the t_{2g} states.

In the case of the 6 nm thick $\text{Sr}_3\text{Ru}_2\text{O}_7$ film deposited on STO [Fig. 2(c)], the measured FSs closely resemble those of $\text{Sr}_3\text{Ru}_2\text{O}_7$ in the ideal tetragonal structure [13]. This corresponds to the situation whereby, the FS analogous to that of the monolayer Sr_2RuO_4 , reconstructs due to the interaction of the RuO_2 sheets within the bilayer and their subsequent splitting and hybridization. The FS consists of two Γ -centered electron-like pockets [13, 54] and a broad feature at Γ . Although the orbital character of the latter is not yet firmly established, the former are believed to arise from an even combination of d_{xz} and d_{yz} orbitals [13].

The DFT results [Fig. 2(d)] show striking agreement with the ARPES measurements. The calculations assume that the in-plane Ru–O geometry is identical in the top and bottom layers, indicating no relative in-plane rotation of the RuO_6 octahedra. This agreement suggests that, in the epitaxial bilayer $\text{Sr}_3\text{Ru}_2\text{O}_7$ films, the electronic structure is predominantly determined by the Ru–O bonding geometry within each layer, while interlayer coupling and the thin-film constraints imposed by the substrate preserve the in-plane octahedral symmetry [57]. The absence of relative octahedral rotation or tilt implies minimal structural distortion, allowing the DFT calculations to accurately reproduce the measured FS features. Importantly, this highlights a thin-

film effect: under epitaxial constraints, the octahedral network remains in a high-symmetry configuration, suppressing distortions or rotation patterns that could otherwise break symmetry, an effect not necessarily present in bulk crystals of similar composition.

The ARPES-measured FSs reveal substrate-dependent modifications that reflect the underlying strain states of the films. The tensile strain imposed by the STO substrate largely preserves tetragonal symmetry, whereas the compressive strain from the LSAT substrate reduces the symmetry and induces an orthorhombic phase. These structural differences, including the resulting fourfold rotation symmetries around Γ , are well captured by the DFT calculations. Notably, while orthorhombic systems do not strictly possess fourfold symmetry, our observations remain consistent with previous ARPES and DFT studies on $\text{Sr}_3\text{Ru}_2\text{O}_7$ single crystals [26, 54], indicating that the bilayer and substrate constraints dominate the observed electronic structure. Another important consideration is the low temperature at which the ARPES measurements are performed, as both LSAT and STO substrates are known to undergo symmetry changes that could, in principle, influence the film structure in addition to strain effects [58, 59]. However, the presence of orthorhombic and tetragonal symmetries at room temperature can be directly inferred from reciprocal space mapping (RSM) measurements, reducing the likelihood that the observed structural changes arise from temperature-driven substrate transitions or interfacial coupling effects. To further corroborate the strain-driven structural distortions inferred from ARPES and DFT, the octahedral rotation patterns can be identified through half-integer reflections measured using synchrotron-based XRD, which are particularly sensitive to strain states and interfacial coupling [49–53]. Such measurements, however, are beyond the scope of the present study.

It is worth highlighting an interesting contrast between our measured and calculated FSs. This is the absence of the predicted innermost δ pocket in the orthorhombic

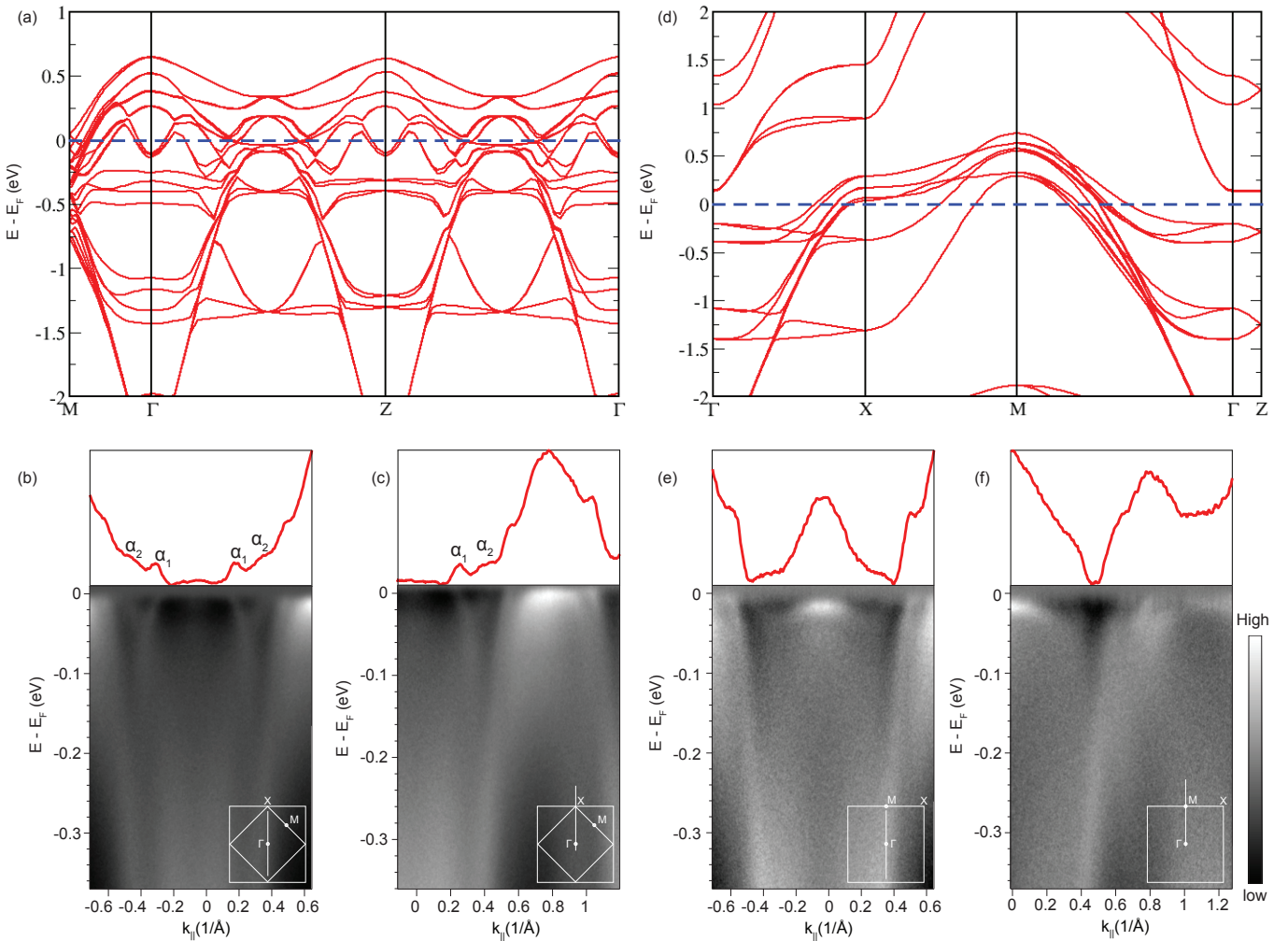


FIG. 3. (a) DFT-calculated band structure of $\text{Sr}_3\text{Ru}_2\text{O}_7$ grown on LSAT, including the folded bands for an orthorhombic phase. (b) and (c) ARPES-measured band dispersions of $\text{Sr}_3\text{Ru}_2\text{O}_7$ on LSAT along the Γ -X direction at two different manipulator angles, sampling distinct regions of the Brillouin zone. The MDC at E_F are overlaid (red curves). (d) DFT-calculated band structure of $\text{Sr}_3\text{Ru}_2\text{O}_7$ grown on STO. (e) and (f) ARPES-measured band structure of $\text{Sr}_3\text{Ru}_2\text{O}_7$ on STO along two momentum regions. The insets in (b), (c), (e), and (f) indicates the momentum-cut locations in the Brillouin zone. To visualize the edges of the narrow features around E_F in (c) and (e), we performed their first derivatives as shown in the supplementary information.

phase, and the presence of an unexpected flat band feature at Γ in the tetragonal phase. This is clearly laid out in Fig. 3, which shows the measured and calculated energy band dispersions along high symmetry directions. In the orthorhombic phase [Fig. 3(a) to 3(c)], the momentum distribution curves (MDCs) extracted at E_F show no sign of dispersing feature around Γ , while the band structure calculation shows two distinct Γ centered bands crossing E_F . These are bilayer splittings of the δ pocket [13]. They are unresolved in ARPES most likely because of their intrinsically low spectral weight, which in thin films can be further suppressed by disorder, reduced coherence, and matrix-element effect [26]. In the tetragonal phase on the other hand [Fig. 3(d) to 3(f)], the MDCs show a flat band near E_F centered at Γ , but no band dispersion crossing E_F is seen in the calcula-

tion at Γ . Instead, four nearly degenerate bands are observed well below E_F . These are bonding-anti bonding splittings of the d_{xz} and d_{yz} states associated with the interbilayer interaction.

Note that the flat spectral weight character of the feature around $0.6 - 0.9 \text{ \AA}^{-1}$ along Γ X in the orthorhombic phase [Fig. 3(c)] and that of the band at Γ in the tetragonal phase [Fig. 3(e)] is consistent with the low-energy flat band reported in Ref. [60]. This is also confirmed through visualization of their edges [see supplemental information]. Owing to the proximity of these bands to E_F (≈ 15 meV below E_F), it could happen that nearby van Hove singularities occur and subsequently drive a metamagnetic instability in the $\text{Sr}_3\text{Ru}_2\text{O}_7$ films when tuned by an applied magnetic field. This hypothesis, on the other hand, would require further validation through transport

and specific-heat measurements, as both probes can reveal signatures of enhanced scattering and increased features in the DOS in the vicinity of the metamagnetic transition [18, 19, 24, 61].

Even with an energy resolution of 5 meV, resolving the finest band features in $\text{Sr}_3\text{Ru}_2\text{O}_7$ thin films remains experimentally demanding. As discussed above, this behavior is consistent with modest quasiparticle linewidth broadening that can arise from surface roughness and other near-surface disorder inherent to complex oxide thin films [62]. While these effects currently limit a direct experimental identification of all FS pockets observed in bulk $\text{Sr}_3\text{Ru}_2\text{O}_7$ single crystals [26], the overall agreement between ARPES and DFT demonstrates that the essential low-energy electronic structure is well captured in the thin-film geometry. Looking forward, high-resolution synchrotron-based ARPES measurements, combined with controlled light polarization (linear horizontal and linear vertical) [63], are expected to further enhance orbital selectivity and sensitivity to narrow features near E_F , providing a promising pathway toward resolving finer details of the electronic structure in $\text{Sr}_3\text{Ru}_2\text{O}_7$ thin films.

In conclusion, we have performed the first *in-situ* ARPES investigation of $\text{Sr}_3\text{Ru}_2\text{O}_7$ thin films. For controlled strain engineering, we have prepared the $\text{Sr}_3\text{Ru}_2\text{O}_7$ films on LSAT and STO to insure respectively compressive and tensile strains in the films. Upon ARPES measurements of the FSs, we found that the compressive strain promotes RuO_6 octahedral rotations and leads to an orthorhombic symmetry, whereas the tensile strain retains a more symmetric, tetragonal-like structure. These observations are supported by the DFT calculations which implement the intrinsic structural characteristics of the grown samples. The ARPES measured band dispersions present narrow flat band features about 15 meV below E_F . These bands could potentially be favorable for van Hove singularities and subsequently drive magnetic instabilities in the epitaxial $\text{Sr}_3\text{Ru}_2\text{O}_7$ films. Our results underscore the strong sensitivity of the electronic structure of $\text{Sr}_3\text{Ru}_2\text{O}_7$ to epitaxial strain and establish a foundation for future efforts to tune correlated phases in this bilayer ruthenate.

ACKNOWLEDGEMENTS

P. N., S. S., and A. N. T. acknowledge funding from the College of Science and the Department of Physics & Astronomy at Louisiana State University. This work made use of the synthesis facility of the Platform for the Accelerated Realization, Analysis, and Discovery of Interface Materials (PARADIM), which is supported by the National Science Foundation under Cooperative Agreement No. DMR-2039380.

DATA AVAILABILITY

The data that support the findings are available from the authors upon reasonable request.

* corresponding author: pngabonziza@lsu.edu

- [1] G. M. Luke, Y. Fudamoto, K. M. Kojima, M. I. Larkin, B. Nachumi, Y. J. Uemura, J. E. Sonier, Y. Maeno, Z. Q. Mao, Y. Mori, and D. F. Agterberg, Unconventional superconductivity in Sr_2RuO_4 , *Physica B* **289–290**, 373 (2000).
- [2] R. S. Russell, H. P. Nair, K. M. Shen, D. G. Schlom, and J. W. Harter, Electronic nematic order in the normal state of strontium ruthenate, *Phys. Rev. B* **108**, L081105 (2023).
- [3] R. S. Perry, T. Tayama, K. Kitagawa, T. Sakakibara, K. Ishida, and Y. Maeno, Investigation into the itinerant metamagnetism of $\text{Sr}_3\text{Ru}_2\text{O}_7$ for the field parallel to the ruthenium-oxygen planes, *J. Phys. Soc. Jpn.* **74**, 1270 (2005).
- [4] E. Carleschi, B. P. Doyle, R. Fittipaldi, V. Granata, A. M. Strydom, M. Cuoco, and A. Vecchione, Double metamagnetic transition in $\text{Sr}_4\text{Ru}_3\text{O}_{10}$, *Phys. Rev. B* **90**, 205120 (2014).
- [5] S. N. Bushmeleva, V. Y. Pomjakushin, E. V. Pomjakushina, D. V. Sheptyakov, and A. M. Balagurov, Evidence for band ferromagnetism in SrRuO_3 from neutron diffraction, *J. Magn. Magn. Mater.* **305**, 491 (2006).
- [6] A. Putatunda, G. Qin, W. Ren, and D. J. Singh, Competing magnetic orders in quantum critical $\text{Sr}_3\text{Ru}_2\text{O}_7$, *Phys. Rev. B* **102**, 014442 (2020).
- [7] P. Ngabonziza, J. D. Denlinger, A. V. Fedorov, G. Cao, J. W. Allen, G. Gebreyesus, and R. M. Martin, Layer-dependent spin-resolved electronic structure of ferromagnetic triple-layered ruthenate $\text{Sr}_4\text{Ru}_3\text{O}_{10}$, *Phys. Rev. B* **111**, 115146 (2025).
- [8] T.-C. Wei, H.-P. Wang, H.-J. Liu, D.-S. Tsai, J.-J. Ke, C.-L. Wu, Y.-P. Yin, Q. Zhan, G.-R. Lin, Y.-H. Chu, and J.-H. He, Photostriction of strontium ruthenate, *Nat. Commun.* **8**, 15018 (2017).
- [9] J. Peng, Z. Qu, B. Qian, D. Fobes, T. Liu, X. Wu, H. M. Pham, L. Spinu, and Z. Q. Mao, Interplay between the lattice and spin degrees of freedom in $(\text{Sr}_{1-x}\text{Ca}_x)_3\text{Ru}_2\text{O}_7$, *Phys. Rev. B* **82**, 024417 (2010).
- [10] S.-I. Ikeda, Y. Maeno, S. Nakatsuji, M. Kosaka, and Y. Uwatoko, Ground state in $\text{Sr}_3\text{Ru}_2\text{O}_7$: Fermi liquid close to a ferromagnetic instability, *Phys. Rev. B* **62**, R6089 (2000).
- [11] Q. Huang, J. W. Lynn, R. W. Erwin, J. Jarupatrakorn, and R. J. Cava, Oxygen displacements and search for magnetic order in $\text{Sr}_3\text{Ru}_2\text{O}_7$, *Phys. Rev. B* **58**, 8515 (1998).
- [12] H. Shaked, J. D. Jorgensen, O. Chmaissem, S. Ikeda, and Y. Maeno, Neutron diffraction study of the structural distortions in $\text{Sr}_3\text{Ru}_2\text{O}_7$, *J. Solid State Chem.* **154**, 361 (2000).
- [13] D. J. Singh and I. I. Mazin, Electronic structure and magnetism of $\text{Sr}_3\text{Ru}_2\text{O}_7$, *Phys. Rev. B* **63**, 165101 (2001).
- [14] B. Hu, G. T. McCandless, M. Menard, V. B. Nascimento, J. Y. Chan, E. W. Plummer, and R. Jin, Surface and

bulk structural properties of single-crystalline $\text{Sr}_3\text{Ru}_2\text{O}_7$, *Phys. Rev. B* **81**, 184104 (2010).

[15] R. Kiyanagi, K. Tsuda, N. Aso, H. Kimura, Y. Noda, Y. Yoshida, S.-I. Ikeda, and Y. Uwatoko, Investigation of the structure of single-crystal $\text{Sr}_3\text{Ru}_2\text{O}_7$ by neutron and convergent beam electron diffractions, *J. Phys. Soc. Jpn.* **73**, 639 (2004).

[16] C. Lester, S. Ramos, R. S. Perry, T. P. Croft, M. Laver, R. I. Bewley, T. Guidi, A. Hiess, A. Wildes, E. M. Forgan, and S. M. Hayden, Magnetic-field-controlled spin fluctuations and quantum criticality in $\text{Sr}_3\text{Ru}_2\text{O}_7$, *Nat. Commun.* **12**, 5798 (2021).

[17] S. A. Grigera, R. S. Perry, A. J. Schofield, M. Chiao, S. R. Julian, G. G. Lonzarich, S. I. Ikeda, Y. Maeno, A. J. Millis, and A. P. Mackenzie, Magnetic field-tuned quantum criticality in the metallic ruthenate $\text{Sr}_3\text{Ru}_2\text{O}_7$, *Science* **294**, 329 (2001).

[18] R. S. Perry, L. M. Galvin, S. A. Grigera, L. Capogna, A. J. Schofield, A. P. Mackenzie, M. Chiao, S. R. Julian, S. I. Ikeda, S. Nakatsuji, Y. Maeno, and C. Pfleiderer, Metamagnetism and critical fluctuations in high quality single crystals of the bilayer ruthenate $\text{Sr}_3\text{Ru}_2\text{O}_7$, *Phys. Rev. Lett.* **86**, 2661 (2001).

[19] A. W. Rost, S. A. Grigera, J. A. N. Bruin, R. S. Perry, D. Tian, S. Raghu, S. A. Kivelson, and A. P. Mackenzie, Thermodynamics of phase formation in the quantum critical metal $\text{Sr}_3\text{Ru}_2\text{O}_7$, *Proc. Natl. Acad. Sci. U.S.A.* **108**, 16549 (2011).

[20] C. H. Mousatov, E. Berg, and S. A. Hartnoll, Theory of the strange metal $\text{Sr}_3\text{Ru}_2\text{O}_7$, *Proc. Natl. Acad. Sci. U.S.A.* **117**, 2852 (2020).

[21] A. Millis, A. Schofield, G. Lonzarich, and S. Grigera, Metamagnetic quantum criticality in metals, *Phys. Rev. Lett.* **88**, 217204 (2002).

[22] P. Gegenwart, F. Weickert, M. Garst, R. Perry, and Y. Maeno, Metamagnetic quantum criticality in $\text{Sr}_3\text{Ru}_2\text{O}_7$ studied by thermal expansion, *Phys. Rev. Lett.* **96**, 136402 (2006).

[23] R. Z. Levitin and A. S. Markosyan, Itinerant metamagnetism, *Soviet Physics Uspekhi* **31**, 730 (1988).

[24] B. Binz and M. Sigrist, Metamagnetism of itinerant electrons in multi-layer ruthenates, *Europhys. Lett.* **65**, 816 (2004).

[25] T. Sakakibara, T. Goto, K. Yoshimura, and K. Fukamichi, Itinerant electron metamagnetism and spin fluctuations in nearly ferromagnetic metals $\text{Y}(\text{Co}_{1-x}\text{Al}_x)_2$, *J. Phys.: Condens. Matter* **2**, 3381 (1990).

[26] A. Tamai, M. P. Allan, J. F. Mercure, W. Meevasana, R. Dunkel, D. H. Lu, R. S. Perry, A. P. Mackenzie, D. J. Singh, Z.-X. Shen, and F. Baumberger, Fermi surface and van hove singularities in the itinerant metamagnet $\text{Sr}_3\text{Ru}_2\text{O}_7$, *Phys. Rev. Lett.* **101**, 026407 (2008).

[27] J. Lee, M. P. Allan, M. A. Wang, J. Farrell, S. A. Grigera, F. Baumberger, J. C. Davis, and A. P. Mackenzie, Heavy d-electron quasiparticle interference and real-space electronic structure of $\text{Sr}_3\text{Ru}_2\text{O}_7$, *Nat. Phys.* **5**, 800 (2009).

[28] M. P. Allan, A. Tamai, E. Rozbicki, M. H. Fischer, J. Voss, P. D. C. King, W. Meevasana, S. Thirupathaiah, E. Rienks, J. Fink, D. A. Tennant, R. S. Perry, J. F. Mercure, M. A. Wang, J. Lee, C. J. Fennie, E.-A. Kim, M. J. Lawler, K. M. Shen, A. P. Mackenzie, Z.-X. Shen, and F. Baumberger, Formation of heavy d-electron quasiparticles in $\text{Sr}_3\text{Ru}_2\text{O}_7$, *New J. Phys.* **15**, 063029 (2013).

[29] P. B. Marshall, K. Ahadi, H. Kim, and S. Stemmer, Electron nematic fluid in a strained $\text{Sr}_3\text{Ru}_2\text{O}_7$ film, *Phys. Rev. B* **97**, 155160 (2018).

[30] D. O. Brodsky, M. E. Barber, J. A. N. Bruin, R. A. Borzi, S. A. Grigera, R. S. Perry, A. P. Mackenzie, and C. W. Hicks, Strain and vector magnetic field tuning of the anomalous phase in $\text{Sr}_3\text{Ru}_2\text{O}_7$, *Sci. Adv.* **3**, e1501804 (2017).

[31] S. Mukherjee and W.-C. Lee, Structural and magnetic field effects on spin fluctuations in $\text{Sr}_3\text{Ru}_2\text{O}_7$, *Phys. Rev. B* **94**, 064407 (2016).

[32] H. Yamase and A. A. Katanin, Van hove singularity and spontaneous fermi surface symmetry breaking in $\text{Sr}_3\text{Ru}_2\text{O}_7$, *J. Phys. Soc. Jpn.* **76**, 073706 (2007).

[33] D. V. Efremov, A. Shtyk, A. W. Rost, C. Chamon, A. P. Mackenzie, and J. J. Betouras, Multicritical fermi surface topological transitions, *Phys. Rev. Lett.* **123**, 207202 (2019).

[34] Y. Tokiwa, M. McHalwat, R. S. Perry, and P. Gegenwart, Multiple metamagnetic quantum criticality in $\text{Sr}_3\text{Ru}_2\text{O}_7$, *Phys. Rev. Lett.* **116**, 226402 (2016).

[35] Z. Liu, C. Menéndez, J. Shenoy, J. N. Hart, C. C. Sorrell, and C. Cazorla, Strain engineering of oxide thin films for photocatalytic applications, *Nano Energy* **72**, 104732 (2020).

[36] K. Terai, T. Ohnishi, M. Lippmaa, *et al.*, Magnetic properties of strain-controlled SrRuO_3 thin films, *Jpn. J. Appl. Phys.* **43**, L227 (2004).

[37] J. Du, H. Yu, B. Liu, M. Hong, Q. Liao, Z. Zhang, and Y. Zhang, Strain engineering in 2d material-based flexible optoelectronics, *Small Methods* **5**, 2000919 (2021).

[38] R. Choudhary, A. Rajapitamahuni, S. Guo, Q. Jiang, J.-H. Chu, K. A. Mkhoyan, and B. Jalan, Intrinsic vs. extrinsic magnetic transitions in $\text{Sr}_3\text{Ru}_2\text{O}_7$ films, *J. Mater. Res.* **40**, 2351 (2025).

[39] J. Choi, C.-B. Eom, G. Rijnders, H. Rogalla, and D. H. Blank, Growth mode transition from layer by layer to step flow during the growth of heteroepitaxial SrRuO_3 on (001) SrTiO_3 , *Appl. Phys. Lett.* **79**, 1447 (2001).

[40] W. Tian, J. Haeni, D. G. Schlom, E. Hutchinson, B. Sheu, M. Rosario, P. Schiffer, Y. Liu, M. A. Zurbuchen, and X. Pan, Epitaxial growth and magnetic properties of the first five members of the layered $\text{Sr}_{n+1}\text{Ru}_n\text{O}_{3n+1}$ oxide series, *Appl. Phys. Lett.* **90**, <https://doi.org/10.1063/1.2430941> (2007).

[41] J. H. Haeni, P. Irvin, W. Chang, R. Uecker, P. Reiche, Y. L. Li, S. Choudhury, W. Tian, M. E. Hawley, B. Craig, A. K. Tagantsev, X. Q. Pan, S. K. Streiffer, L. Q. Chen, S. W. Kirchoefer, J. Levy, and D. G. Schlom, Room-temperature ferroelectricity in strained SrTiO_3 , *Nat.* **430**, 758 (2004).

[42] R. Kiyanagi, K. Tsuda, N. Aso, H. Kimura, Y. Noda, Y. Yoshida, S.-I. Ikeda, and Y. Uwatoko, Investigation of the structure of single-crystal $\text{Sr}_3\text{Ru}_2\text{O}_7$ by neutron and convergent beam electron diffractions, *J. Phys. Soc. Jpn.* **73**, 639 (2004).

[43] G. Gebreyesus, P. Ngabonziza, J. Nagura, N. Seriani, O. Akin-Ojo, and R. M. Martin, Electronic structure and magnetism of the triple-layered ruthenate $\text{Sr}_4\text{Ru}_3\text{O}_{10}$, *Physical Review B* **105**, 165119 (2022).

[44] E. N. Kaufmann, *Characterization of Materials* (John Wiley & Sons, Inc., Hoboken, NJ, 2012).

[45] H. Paik, Z. Chen, E. Lochocki, A. H. Seidner, A. Verma, N. Tanen, J. Park, M. Uchida, S. Shang, B.-C. Zhou,

M. Brützam, R. Uecker, Z.-K. Liu, D. Jena, K. M. Shen, D. A. Muller, and D. G. Schlom, Adsorption-controlled growth of la-doped BaSnO₃ by molecular-beam epitaxy, *APL Mater.* **5**, 116107 (2017).

[46] A. M. Miller, M. Lemon, M. A. Choffel, S. R. Rich, F. Harvel, and D. C. Johnson, Extracting information from x-ray diffraction patterns containing laue oscillations, *Zeitschrift für Naturforschung B* **77**, 313 (2022).

[47] Y. K. Wakabayashi, S. Kaneta-Takada, Y. Krockenberger, Y. Taniyasu, and H. Yamamoto, Wide-range epitaxial strain control of electrical and magnetic properties in high-quality SrRuO₃ films, *ACS Appl. Electron. Mater.* **3**, 2712 (2021).

[48] P. Ngabonziza, A. Sharma, A. Scheid, S. Sajeev, P. A. van Aken, and J. Mannhart, Magnetotransport properties of epitaxial films and hall bar devices of the correlated layered ruthenate Sr₃Ru₂O₇, *Physical Review Materials* **8**, 044401 (2024).

[49] A. Vailionis, H. Boschker, W. Siemons, E. P. Houwman, D. H. A. Blank, G. Rijnders, and G. Koster, Misfit strain accommodation in epitaxial ABO₃ perovskites: Lattice rotations and lattice modulations, *Phys. Rev. B* **83**, 064101 (2011).

[50] W. Lu, W. Song, P. Yang, J. Ding, G. M. Chow, and J. Chen, Strain engineering of octahedral rotations and physical properties of SrRuO₃ films, *Sci. Rep.* **5**, 10245 (2015).

[51] A. M. Glazer, The classification of tilted octahedra in perovskites, *Acta Crystallogr. B* **28**, 3384 (1972).

[52] D. Kan, M. Anada, Y. Wakabayashi, H. Tajiri, and Y. Shimakawa, Oxygen octahedral distortions in compressively strained SrRuO₃ epitaxial thin films, *J. Appl. Phys.* **123**, 235303 (2018).

[53] W. Lu, P. Yang, W. Song, G. M. Chow, and J. Chen, Control of oxygen octahedral rotations and physical properties in SrRuO₃ films, *Phys. Rev. B* **88**, 214115 (2013).

[54] A. V. Puchkov, Z.-X. Shen, and G. Cao, Electronic band structure of Sr₃Ru₂O₇, *Phys. Rev. B* **58**, 6671 (1998).

[55] C. Li, M. Hu, J. Zhang, M. H. Berntsen, F. Scali, D. Phuyal, C. Lin, W. Chen, J. Chang, O. J. Clark, *et al.*, Extreme strain controlled correlated metal-insulator transition in the altermagnet CrSb, arXiv:2512.07683 <https://doi.org/10.48550/arXiv.2512.07683> (2025).

[56] C. Rayan Serrao, J. Liu, J. Heron, G. Singh-Bhalla, A. Yadav, S. Suresha, R. Paull, D. Yi, J.-H. Chu, M. Trassin, *et al.*, Epitaxy-distorted spin-orbit mott insulator in Sr₂IrO₄ thin films, *Phys. Rev. B* **87**, 085121 (2013).

[57] R. Gao, Y. Dong, H. Xu, H. Zhou, Y. Yuan, V. Gopalan, C. Gao, D. D. Fong, Z. Chen, Z. Luo, *et al.*, Interfacial octahedral rotation mismatch control of the symmetry and properties of SrRuO₃, *ACS Appl. Mater. Interfaces* **8**, 14871 (2016).

[58] B. C. Chakoumakos, D. G. Schlom, M. Urbanik, and J. Luine, Thermal expansion of LaAlO₃ and (La,Sr)(Al,Ta)O₃, substrate materials for superconducting thin-film device applications, *J. Appl. Phys.* **83**, 1979 (1998).

[59] N. V. Krainyukova, V. O. Hamalii, A. V. Peschanskii, A. I. Popov, and E. A. Kotomin, Low temperature structural transformations on the (001) surface of SrTiO₃ single crystals, *Low Temperature Physics* **46**, 740 (2020).

[60] D. Oh, A. Hampel, J. P. Wakefield, P. C. Moen, S. Smit, X. Luo, M. Zonno, S. Gorovikov, M. Leandersson, C. Polley, *et al.*, Hund's flat band in a frustrated spinel oxide, *Proc. Natl. Acad. Sci.* **122**, e2518213122 (2025).

[61] H. Yamase and A. A. Katanin, Theory of spontaneous fermi surface symmetry breaking for Sr₃Ru₂O₇, *Phys. Rev. B Condens. Matter* **403**, 1262 (2008).

[62] E. Della Valle, P. Constantinou, T. Schmitt, G. Aeppli, and V. N. Strocov, Static disorder in soft x-ray angle-resolved photoemission spectroscopy: theory and application to ion-bombarded InAs (110), arXiv preprint <https://doi.org/10.48550/arXiv.2512.07683> (2023).

[63] P. Ngabonziza, E. Carleschi, V. Zabolotnyy, A. Taleb-Ibrahimi, F. Bertran, R. Fittipaldi, V. Granata, M. Cuoco, A. Vecchione, and B. P. Doyle, Fermi surface and kink structures in Sr₄Ru₃O₁₀ revealed by synchrotron-based arpes, *Sci. Rep.* **10**, 21062 (2020).

Supplementary Information:

Electronic Structure of Epitaxial Films of the Bilayer Strontium Ruthenate: $\text{Sr}_3\text{Ru}_2\text{O}_7$

Sethulakshmi Sajeev¹, Arnaud P. Nono Tchiomo¹, Brendon Faeth^{2,3}, Evan Cryska^{2,3}, Olivia Peek^{2,4}, Matthew J. Barone^{2,3}, Jordan Shields⁵, Neha Wadehra^{2,3}, Garu Gebreyesus⁶, Divine Kumah⁵, Richard M. Martin⁷, Darrell G. Schlom^{2,3} and Prosper Ngabonziza^{1,8}

¹*Department of Physics and Astronomy, Louisiana State University, Baton Rouge, LA 70803, USA*

²*Platform for the Accelerated Realization, Analysis, and Discovery of Interface Materials(PARADIM), Cornell University, Ithaca, New York, 14853, USA*

³*Department of Material science and engineering, Cornell University, Ithaca, New York, 14853, USA*

⁴*Department of Physics, Cornell University, Ithaca, New York, 14853, USA*

⁵*Department of Physics, Duke University, Durham, North Carolina, USA*

⁶*Department of Physics, College of Basic and Applied Sciences, University of Ghana, Ghana*

⁷*Department of Applied Physics, Stanford University, Stanford, California 94305, USA*

⁸*Department of Physics, University of Johannesburg, P.O. Box 524 Auckland Park 2006, Johannesburg, South Africa*

Derivatives of the ARPES data

To visualize the edges of the bands around E_F in the ARPES data, we performed the first derivative of the raw ARPES maps presented in Fig.3(c) and 3(e) of the main text. Taking the derivatives enhances resolution of narrow bands and helps in identifying key features including flat bands and inflection points. It describes how the slope changes with respect to energy or momentum. In the figure below, we present the first derivative with respect to the energy axis as well as to the momentum axis to highlight the flat band features.

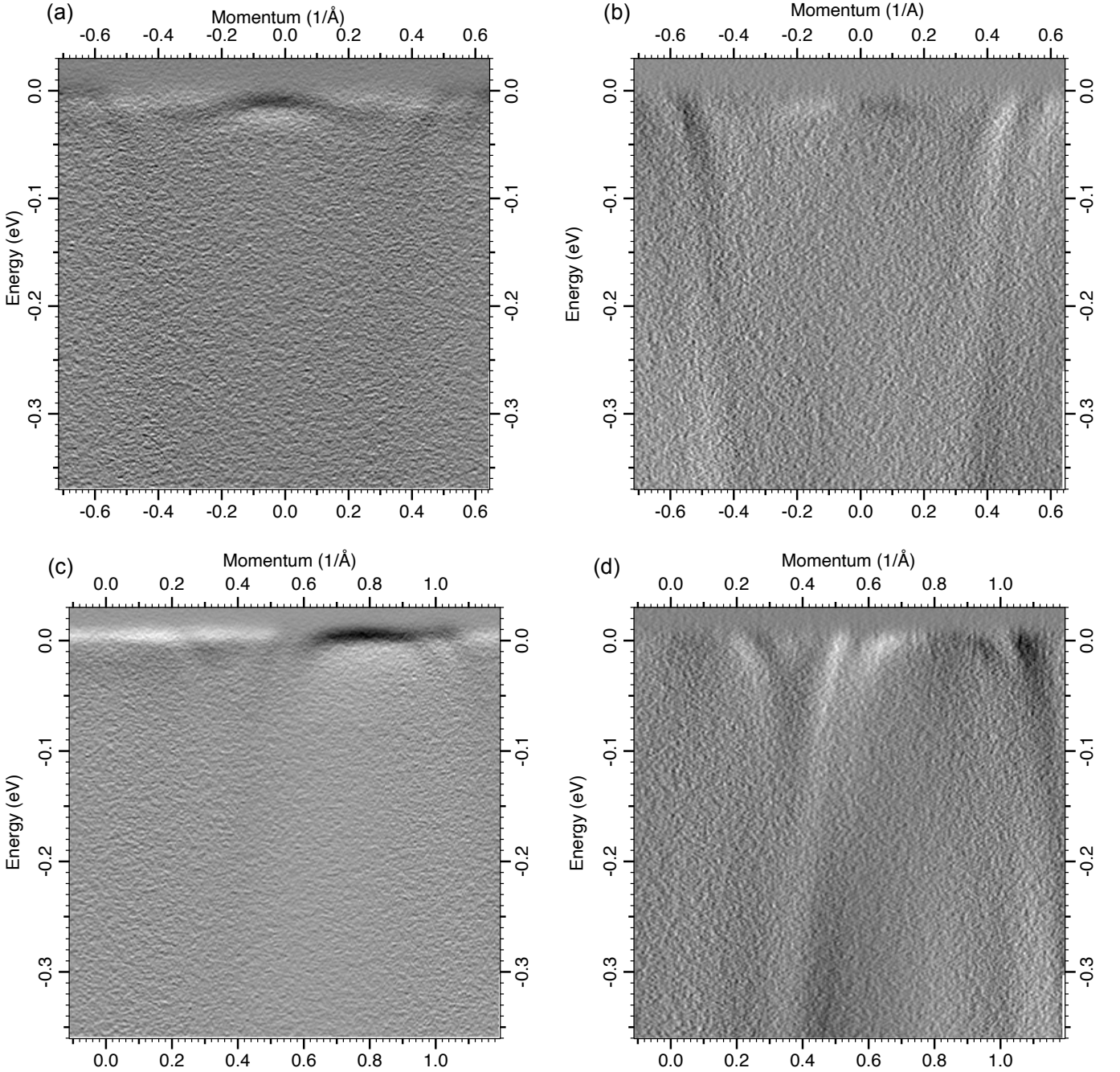


FIG. S1. Figure S1: First derivatives of the original ARPES maps of the $\text{Sr}_3\text{Ru}_2\text{O}_7$ thin films plotted in Fig 3(c) and 3(e) of the main text. (a) and (b) are the data of the film deposited on STO [Fig 3(e) of the main text]. (a) represent the derivative with respect to the energy dimension, and (b) is that along the momentum axis. The edges of the nearly narrow feature located about 15 meV below E_F and centered at Γ are visible in (a). This feature seems to have been completely quenched when the derivative is applied along the momentum direction, attesting to its nearly flat character [1]. (c) and (d) are the data for the film prepared on LSAT [Fig 3(c) of the main text]. Similarly, the edges of a flat band around $0.6\text{--}0.9 \text{ \AA}^{-1}$ are visible when the derivative is performed with respect to the energy axis in (c). Only steep bands are visible in (d), when the derivative is performed along the momentum axis.

References

[1] Yong Hu, Xianxin Wu, Brenden R. Ortiz, Sailong Ju, Xinloong Han, Junzhang Ma, Nicholas C. Plumb, Milan Radovic, Ronny Thomale, Stephen D. Wilson, Andreas P. Schnyder, and Ming Shi, *Nature Commun.* **13**, 2220 (2022).